

# Overpressure, vertical stress, compaction and horizontal loading along the North Alpine Thrust Front, SE Germany

Michael C. Drews<sup>a,\*</sup>, Florian Duschl<sup>a</sup>

<sup>a</sup> Technical University of Munich, Arcisstraße 21, 80333 Munich, Germany

## ARTICLE INFO

### Keywords:

Subalpine molasse  
Molasse basin  
North alpine foreland basin  
Fold-and-thrust-belt  
Pore pressure  
Disequilibrium compaction

## ABSTRACT

The North Alpine Thrust Front divides the outer wedge of the northern Alps from its foredeep, the North Alpine Foreland Basin, representing a classic fold-and-thrust-belt system. In its SE German part, this system is characterized by a complex pore pressure distribution, which we investigate to better understand the impact of horizontal loading (tectonic stress) on sediment compaction, vertical stress and overpressure formation. To do so, we analyze velocity, pore pressure and drilling data of 20 deep wellbores along both sides of the North Alpine Thrust Front. Our results indicate that overpressure in the wedge is largely driven syntectonically by horizontal loading, while vertical loading appears to be the main overpressure mechanism not only in the foredeep but also in the footwall of the wedge. Here, pore fluids can support up to 90% or even more of the overburden weight. Still, the lateral transition zone from horizontal to vertical loading conditions likely comprises only a few kilometers. Our study provides real-world evidence of the complex processes of overpressure development in onshore fold-and-thrust-belts and helps to mitigate pore pressure related drilling and exploration risks along the North Alpine Thrust Front in SE Germany.

## 1. Introduction

Geological processes such as deformation, subsidence, fault slip and related earthquakes as well as fluid migration critically depend on the distribution of pressure and stress in the subsurface (Allen and Allen, 2013; Zoback, 2007). Likewise, planning and operation of safe drilling campaigns, fluid production and injection, and waste storage require an in-depth understanding of the distribution of subsurface pressure and stresses (Fjaer et al., 2008; Zoback, 2007). This is in particular valid, if pore pressure exceeds normal hydrostatic pressure, resulting in overpressured formations, which can significantly reduce the mechanical integrity of the subsurface (Suppe, 2014).

In most sediments, overpressure primarily forms as a result of rapid loading rates, which exceed sediment dewatering rates (Flemings, 2021; Osborne and Swarbrick, 1997; Swarbrick and Osborne, 1998). As a consequence, the pore fluid cannot escape the pore space during loading, sediment compaction is impeded and the pore pressure increases above a hydrostatic level. This process usually depends on the presence of low permeability formations and is also known as disequilibrium compaction (Flemings, 2021; Osborne and Swarbrick, 1997; Swarbrick and Osborne, 1998). In many areas, such as sedimentary

basins, the loading source would usually be vertically oriented due to rapid burial, while in compressive settings horizontal loading can significantly contribute (Flemings, 2021; Osborne and Swarbrick, 1997; Swarbrick and Osborne, 1998). Horizontal loading also includes shear enhanced compaction. Tectonic compression can also lead to uplift and erosion, both of which – depending on the rate – often dissipate overpressure (Luo and Vasseur, 1995).

In vertical loading-dominated areas, the relationship between vertical effective stress and the compaction-state of clay-rich sediments (shales) has been successfully used to estimate overpressure (e.g. Drews et al., 2018a; Heppard et al., 1998; Merrell et al., 2014). The advantage of this relationship is that it only requires an estimate of vertical stress, e.g. by integrating density data measured in a wellbore, and an understanding of the shale compaction behavior at hydrostatic pore pressure. The relationship between this normal shale compaction behavior and the actual disequilibrium compaction state can then be used to estimate pore pressure and overpressure (e.g. Eaton, 1972; Eaton, 1975; Yang and Aplin, 2004). The compaction state of shales can be determined by porosity-sensitive geophysical measurements, such as seismic/sonic velocity (e.g. Bowers, 1995; Raiga-Clemenceau et al., 1986; Wyllie et al., 1956).

\* Corresponding author.

E-mail address: [michael.c.drews@tum.de](mailto:michael.c.drews@tum.de) (M.C. Drews).

<https://doi.org/10.1016/j.marpetgeo.2022.105806>

Received 21 July 2021; Received in revised form 13 June 2022; Accepted 16 June 2022

Available online 19 June 2022

0264-8172/© 2022 The Authors. Published by Elsevier Ltd. This is an open access article under the CC BY license (<http://creativecommons.org/licenses/by/4.0/>).

In compressive settings, such as fold-and-thrust-belts, sediment compaction and overpressure formation is more complex. Fold-and-thrust-belts usually consist of a deformed wedge which advances over undeformed strata. The latter forms the footwall below the basal detachment of the wedge and transitions into the undeformed foredeep in front of the wedge. Within and directly in front of the wedge, horizontal loading significantly contributes to overpressure formation (Flemings, 2021; Osborne and Swarbrick, 1997; Swarbrick and Osborne, 1998). Here, utilizing vertical effective stress as a proxy for shale compaction will likely result in an underestimation of shale pore pressure (e.g. Couzens-Schultz and Azbel, 2014; Flemings and Saffer, 2018; Obradors-Prats et al., 2017). Nevertheless, vertical loading usually dominates below the basal detachment of fold-and-thrust-belt systems (Byrne and Fisher, 1990; Saffer and Tobin, 2011), which is often evidenced by velocity reversals and a sudden porosity increase (e.g. Bangs et al., 1990; Cochran et al., 1994; Flemings and Saffer, 2018; Saffer and Tobin, 2011; Tsuji et al., 2008). The transition from horizontal loading in the wedge towards vertical loading-dominated far-field conditions is less rapid, but can still comprise only a few kilometers (cf. Flemings and Saffer, 2018; Gao et al., 2018; Obradors-Prats et al., 2017).

An onshore example, representing an overpressured system including a transition from wedge conditions to far-field conditions is given by the northern Alps behind and the North Alpine Foreland Basin (NAFB) in front of the North Alpine Thrust Front (NATF) in SE Germany (cf. Müller and Nieberding, 1996; Müller et al., 1988). The NATF divides the Alpine wedge from its foredeep (NAFB) and thus marks the northern structural outline of the European Alps.

The overpressure distribution along both sides of the NATF has only been addressed on the basis of drilling data of a few wells, yet (Müller and Nieberding, 1996; Müller et al., 1988), whereas the overpressure distribution in the NAFB has been studied in more detail (Drews et al., 2018a, 2018b, 2020b; Müller and Nieberding, 1996; Müller et al., 1988). However, the vertical and lateral distribution of pore pressure and overpressure mechanisms are yet poorly understood in the direct vicinity of the North Alpine Thrust Front. In particular, the impact of tectonic stress (or horizontal loading) compared to vertical stress (or vertical loading) on sediment compaction and hence overpressure formation is unknown. However, preliminary work by Lohr (1969, 1978) showed that seismic velocity in the NAFB increases towards the Alps, possibly as a result of increasing horizontal stress/loading (cf. Lohr, 1978; Müller et al., 1988). Still, the lateral extent of the transition from horizontal loading behind the NATF towards vertical loading in front of the NATF is unclear as evidenced by the controversial discussion of horizontal stress propagation into the foreland (cf. Drews and Stollhofen, 2019; Drews et al., 2018a; Drews et al., 2020b; Reinecker et al., 2010; Ziegler and Heidbach, 2020; Ziegler et al., 2016).

In this study, we analyze the distribution of vertical stress, compaction, overpressure and horizontal loading using velocity, pore pressure and drilling data of 20 deep wellbores, which have been drilled on both sides and in direct vicinity of the North Alpine Thrust Front in SE Germany. The results are set into context with previously published interpretations of 2D seismic data (Müller, 1995; Müller et al., 1988; Ortner et al., 2015; Shipilin et al., 2020) and the relative timing of overpressure development and possible changes of loading mechanisms in the foredeep, wedge and footwall along the NATF will be discussed.

The study provides a unique reference case for overpressure development in onshore fold-and-thrust-belts for specialists working in the fields of geomechanics, structural geology and geodynamics and helps to mitigate pore pressure related drilling and exploration risks along the NATF in SE Germany.

## 2. Representation of pore pressure, vertical stress, vertical effective stress and overpressure

Pore pressure  $u$  and vertical stress  $\sigma_v$  are discussed and displayed as either absolute values in MPa, in combination as vertical effective stress

$\sigma'_v$ , as overpressure  $u^*$  in MPa or in equivalent mud weight representation EMW in this study. The latter has the advantage that it directly relates to the density of the drilling fluid (mud) used to drill deep wellbores. The drilling fluid density (mud weight) is usually adjusted such that the wellbore pressure counterbalances the pore pressure of the drilled formation. Drilling mud weights often only reflect the driller's perception of pore pressure (cf. Drews et al., 2022; Mouchet and Mitchell, 1989), but still provide a valuable overpressure indicator. The equivalent mud weight EMW in g/cm<sup>3</sup> therefore allows for a representation of estimates and measurements of vertical stress and pore pressure in combination with drilling mud weights and calculates as follows:

$$EMW = 1000 \cdot \frac{u}{g^* TVD} \quad (1)$$

where units of the pore pressure  $u$  and the true vertical depth below ground level TVD are in MPa and m, respectively. An EMW > 1.0 g/cm<sup>3</sup> reflects the presence of overpressure and we denote a pore pressure that translates to an EMW of 1.2-1.4 g/cm<sup>3</sup> as mild, 1.4-1.6 g/cm<sup>3</sup> as intermediate, 1.6-1.8 g/cm<sup>3</sup> as high and >1.8 g/cm<sup>3</sup> as very high overpressure.  $u$  can be also replaced by vertical stress  $\sigma_v$  to be represented in EMW.

Vertical effective stress  $\sigma'_v$  is defined as the difference between vertical stress and pore pressure:

$$\sigma'_v = \sigma_v - u \quad (2)$$

and becomes the vertical hydrostatic effective stress  $\sigma'_{v,hyd}$  if  $u$  is the hydrostatic pore pressure exerted by a vertical water column up to ground level.

Overpressure  $u^*$  is defined as the excess pore pressure above hydrostatic pore pressure. Overpressure is also expressed by  $\lambda^*$ , which is the fractional distance between hydrostatic and lithostatic or the fraction of overburden supported by the pore fluid:

$$\lambda^* = \frac{u^*}{\sigma_{v,hyd}} \quad (3)$$

## 3. The North Alpine Thrust Front (NATF) and North Alpine Foreland Basin (NAFB)

The Alpine wedge and NAFB represent a classical onshore fold-and-thrust-belt and foredeep system, divided by the NATF. The system comprises of passive margin sediments on top of crystalline basement and below foredeep sediments, both of which are partly subducted below an advancing wedge (Allen and Allen, 2013; Pfiffner, 1986). The Alpine wedge and NAFB formed as a result of the collision of the European and Adriatic plates at c. 35 Ma (e.g. Pfiffner, 1986; Schmid et al., 2004) and stretches from Geneva, Switzerland, in the West to Lower Austria and into the Carpathian foreland basin and thrust front system in the East. Thereby, the NAFB widens from West to East, reaches its maximum lateral extension in SE Germany (Fig. 1A) before it quickly narrows against the Bohemian Massif as its northeastern boundary (Schmid et al., 2004). Our study area along the NATF is constrained by Lake Constance in the West, the Austrian border in the East (west of Lake Chiemsee and south of the Landshut-Neuötting-High), the Latitude of Munich in the North and the Alpine Nappes in the South (Fig. 1A and B).

### 3.1. Structural-stratigraphic subdivision of the study area

The study area is subdivided into three structural-stratigraphic units (Fig. 2), which, from youngest to oldest, represent the wedge, foredeep and footwall below the wedge and foredeep. The division builds on previous studies by Bachmann and Müller (1996), Bachmann et al. (1987), Kuhlemann and Kempf (2002) and Ortner et al. (2015).

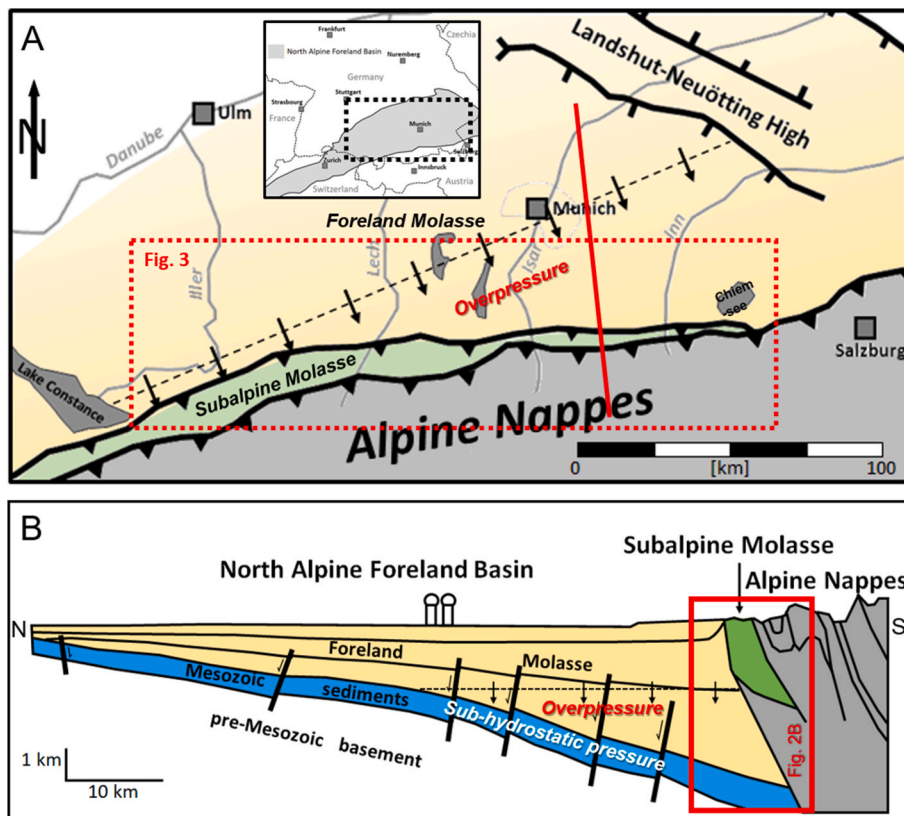


Fig. 1. Overview of the study area. A: Map showing the North Alpine Foreland Basin and North Alpine Thrust Front in SE Germany (modified after Drews et al., 2018a; Reinecker et al., 2010). The black dashed line with southeastwards pointing arrows marks the northwestern border of the overpressure zone in the North Alpine Foreland Basin (cf. Drews et al., 2018a). The inset is indicating the regional position of the study area in southern Germany (modified from Drews et al., 2018a). B: N-S cross-section (red line in Fig. 1A) showing the transition from the Alpine wedge into the North Alpine Foreland Basin (modified from Drews et al., 2018a; Lüschen et al., 2006; Reinecker et al., 2010). (For interpretation of the references to color in this figure legend, the reader is referred to the Web version of this article.)

### 3.1.1. Subalpine Molasse and Alpine Nappes (wedge)

The **Subalpine Molasse** is the outermost tectonic unit of the Alpine wedge (*outer wedge*). It contains deformed and thrust foredeep sediments (Foreland Molasse; Fig. 2A) in front of the **Alpine Nappes** (Fig. 1A and B, Fig. 2B). The Alpine Nappes form the actual thrust sheets of the Alps and are also part of the wedge (*inner wedge*).

The N-S width of the Subalpine Molasse diminishes from West to East in SE Germany and finally tapers out around Lake Chiemsee approximately 30 km westward of the German-Austrian border (Schmid et al., 2004) (Fig. 1A). Thin-skinned thrusting included both, in-sequence-thrusting followed by out-of-sequence thrusting within the Subalpine Molasse (Ortner et al., 2015; Schuller et al., 2015; von Hagke et al., 2014). The former resulted in the formation of a prominent **triangle zone** due to duplex thrusting in the western part of the study area (Ortner et al., 2015) (Fig. 2B). In the eastern part of the Alpine fold-and-thrust-belt and foredeep system in SE Germany, the triangle zone is only weakly expressed or completely missing (Fig. 2B).

### 3.1.2. Foreland Molasse (foredeep and footwall of wedge)

The **Foreland Molasse** is the undeformed foredeep of the Alps filled with Cenozoic Molasse sediments on top of **Mesozoic Passive Margin Sediments**. Cenozoic sedimentation is characterized by two distinct megacycles, each starting in a marine setting and progressing with a subsequent marine regression and shift towards a terrestrial depositional environment (Bachmann and Müller, 1996; Kuhlemann and Kempf, 2002; Sissingh, 1997) (Fig. 2A). During Oligocene times, a geographic transition from a terrestrial depositional environment in the West towards a marine depositional environment in the East is reflected by a decreasing grain size trend from West to East and the presence of brackish-water sediments in the transition zone (Kuhlemann and Kempf, 2002) (Fig. 2A). This grain size trend is also expressed in the Oligocene sediments of the Subalpine Molasse (Ortner et al., 2015). Sheared and subducted Foreland Molasse shales of Oligocene age also form the basal detachment and footwall below the wedge of the Subalpine Molasse and

the Alpine Nappes (Bachmann et al., 1981; Ortner et al., 2015) (Fig. 2A and B).

Close to the wedge, the Foreland Molasse is called **Tilted Molasse**, which is characterized by mostly foreland-dipping Foreland Molasse sediments above the triangle zone of the Subalpine Molasse (Fig. 2B). Analogous to the triangle zone, the Tilted Molasse is only weakly expressed or even missing in the eastern part of the study area (Fig. 2B).

### 3.1.3. Mesozoic passive margin sediments (footwall below foredeep and below wedge)

Autochthonous Mesozoic passive margin sediments of the European plate below the Foreland Molasse are present in the entire study area on top of mostly pre-Mesozoic sediment troughs and Variscan crystalline basement rocks (Fig. 2A). Mesozoic passive margin sediments include Upper Triassic sandstones, Lower and Mid Jurassic shales, Upper Jurassic and Lower Cretaceous carbonates and Upper Cretaceous shales (Bachmann and Müller, 1996; Bachmann et al., 1987). While Upper Jurassic carbonates are present in the entire study area, Lower and Mid Jurassic shales are only present in the central and western part and Cretaceous sediments are only present in the central and eastern parts of the study area. Triassic sandstones are only locally preserved within minor graben systems. Mesozoic passive margin sediments are also subducted below the wedge of the Subalpine Molasse and Alpine Nappes (Fig. 2B). Since the Lower Cretaceous and Upper Jurassic carbonates share the same pressure regime in the NAFB (Drews et al., 2018a, 2020b; Lemcke, 1976) they are summarized as **Mesozoic Passive Margin Carbonates** in this study.

## 3.2. Current understanding of pore pressure along the NATF

Despite the significance of the Subalpine Molasse, Foreland Molasse and Mesozoic passive margin sediments for past hydrocarbon exploration (Bachmann et al., 1981; Lemcke, 1979) and more recent deep geothermal production (Agemar et al., 2014b; Flechtner and Aubele,

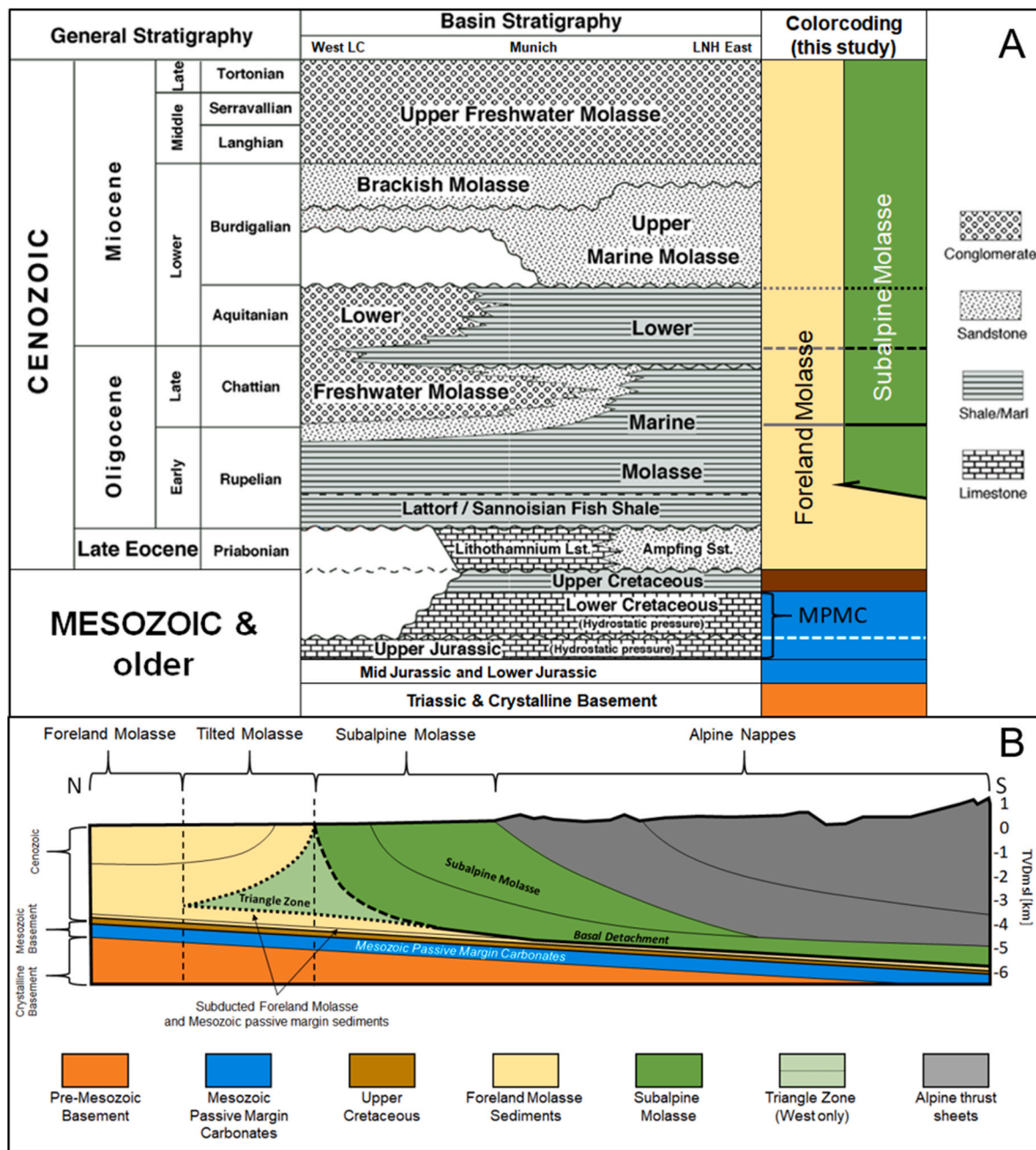


**Fig. 2.** Chronostratigraphic and structural configuration of the northernmost Alpine wedge and North Alpine Foreland Basin. A: Chronostratigraphic chart with color-coding used on maps and cross-sections in this study between Lake Constance (LC) and the Landshut-Neuötting-High (LNH) (cf. Fig. 1A) (modified from Drews et al., 2018a; Drews et al., 2020b; Kuhlmann and Kempf, 2002). MPMC = Mesozoic Passive Margin Carbonates. B: Schematic zoom into the transition from the Foreland Molasse to the Subalpine Molasse with the Tilted Molasse in between (see red rectangle in Fig. 1B for the regional context). The Subalpine Molasse is on top of subducted Foreland Molasse and Mesozoic passive margin sediments (adapted from Ortner et al., 2015). Upper Cretaceous is not present in the western part. The triangle zone (dotted black line, lighter green shading) is missing in the eastern part of the study area (here the dashed black line marks the thrust front). (For interpretation of the references to color in this figure legend, the reader is referred to the Web version of this article.)

2019), few studies addressed the distribution of pore pressure in front of the NATF (Drews et al., 2018a, 2022; Lemcke, 1976; Müller et al., 1988) and behind the NATF (Müller et al., 1988). Overpressure is present in the south and southeast in Foreland Molasse sediments of Oligocene and Eocene age and underlying shales of Late Cretaceous age as evidenced by drilling data and velocity data from wells located in the undeformed foredeep (Drews et al., 2018a; Müller et al., 1988) (Fig. 1A and B). Pore pressure in equivalent mud weight can exceed 1.8 g/cm<sup>3</sup> in the south-eastern part of the NAFB in SE Germany (Drews et al., 2018a; Müller et al., 1988).

Mesozoic Passive Margin Carbonates and underlying formations are

generally hydrostatically pressured or underpressured (Drews et al., 2018a; Lemcke, 1976; Müller et al., 1988) and follow the hydraulic head of the Danube river in the North (Lemcke, 1976). Along the Danube River, the carbonates of the Upper Jurassic are expressed at the surface (Fig. 1A and B).

Within and below the wedge, overpressure is also present; however, it has only been investigated by maximum drilling mud weights (Müller et al., 1988) and exemplarily at a few well locations (Drews and Stollhofen, 2019). Here, pore pressure EMW-magnitudes in excess of 2.0 g/cm<sup>3</sup> have been reported and have mainly been attributed to “tectonic compaction” by Müller et al. (1988) and Müller and Nieberding (1996).

A general increase of compaction and possibly horizontal loading has also been supported by the preliminary work by Lohr (1969, 1978) who noted a general increase of seismic velocities towards the Alps, but did not consider the effect of lithological variation and compaction disequilibrium due to overpressure.

#### 4. Data

The dataset includes 20 wells (sidetracks not counted, Table 1) and 7 cross-sections, which are based on previously published interpretations of seismic sections from Müller (1995), Müller et al. (1988), Ortner et al. (2015) and Shipilin et al. (2020) (Fig. 3). 7 wells are located in the Foreland Molasse, close and along to the NATF; 12 wells have their surface location in the Subalpine Molasse; and one well was drilled through the Alpine Nappes into the Subalpine Molasse (Fig. 3). Four Foreland Molasse wells have reached the Mesozoic Passive Margin Carbonates. Five Subalpine Molasse wells have penetrated the basal detachment and reached at least the subducted part of the Foreland Molasse. The well dataset contains drilling/logging mud weights (19 wells), formation tops (20 wells), cutting descriptions (16 wells), pressure data (13 wells) and velocity data (19 wells).

The data have been derived from geological well reports, the geological division of the Environmental Agency of Bavaria, end of well reports and previously published datasets (Drews et al., 2020b; Müller, 1970, 1995; Müller et al., 1988). Logging mud weights have been retrieved from the headers of geophysical well logs and usually reflect the maximum mud weight used within the logged section. An overview for each well and respective data sources is given in Table 1.

#### 5. Methods

The drilling and velocity dataset are analyzed in four steps to investigate the relationship between overpressure, compaction, vertical and horizontal loading along the NATF in SE Germany:

First, we look at bulk sediment compaction by comparing modelling parameters of velocity-constrained density and vertical stress profiles along each well.

Second, we combine drilling and velocity data to estimate vertical

pore pressure profiles at each well location. The resulting overpressure distribution is investigated on a regional scale in relation to the structural position within, below or in front of the wedge.

Third, shale velocity is analyzed as a function of vertical effective stress to assess the impact of mechanisms other than vertical loading on the compaction state of shales in the different tectonic units along the NATF.

As a fourth and last step, we further delineate the impact of vertical vs horizontal loading on overpressure by considering the structural evolution and related relative timing of overpressure formation in context of the present day overpressure distribution.

##### 5.1. Vertical stress estimation

###### 5.1.1. Vertical stress integration from different data sources

Estimates of vertical stress  $\sigma_v$  are required for both pore pressure and compaction analyses. For reasons of simplicity, we assume that vertical stress is a principal stress component of the stress tensor in the entire study area. Vertical stress can be estimated by integrating the weight of the overlying material (e.g. Flemings, 2021; Zoback, 2007):

$$\sigma_v = \int_0^z \rho_{ob}(z)g dz \quad (4)$$

where  $\rho_{ob}$  is the bulk density which varies with depth  $z$  and  $g$  is the Earth's gravitational acceleration at  $9.81 \text{ m/s}^2$ . In this study, depth is always provided as true vertical depth below ground level TVD.

Bulk density  $\rho_{ob}$  is ideally derived from density logs or, in case of missing density data, indirectly from sonic logs or vertical seismic profile (VSP) data. In this study, density data is not available at sufficient quality and quantity and therefore sonic log and VSP data are converted to a density profile by employing Gardner's velocity-density transform (Gardner et al., 1974):

$$\rho_{ob} = 0.23 * (V_p * 3.281)^{0.25} \quad (5)$$

where  $V_p$  is the interval velocity in m/s. When using geophysical well logs, we apply a 30 m moving average filter to smooth and eliminate

**Table 1**

Well data overview with well location and data sources. VSP = vertical seismic profile, GR = gamma ray, DST = drill stem test or production test.

Wellname	Acronym	Easting	Northing	Data (data source)
				Coordinate System: DHDN/GK3
Eberfing 1	Eb	3,667,581	5,296,543	Mud weight (log header), tops, pressure data, cutting descriptions (GWR*), VSP, sonic log, resistivity** (LfU****)
Egling 1 Vtfg	Egl	3,665,817	5,286,457	Mud weight (log header), tops, cutting descriptions (GWR*), sonic log, GR** (LfU****)
Elbsee 1	Elb	3,615,871	5,298,328	Mud weight (log header), tops, cutting descriptions (GWR*), VSP (LfU****)
Endorf 2	End	3,746,448	5,312,219	Mud weight (log header), tops, pressure data, cutting descriptions (GWR*), sonic log, resistivity** (LfU****)
Feilnbach 1	Fei	3,725,731	5,297,775	Mud weight (log header), tops, pressure data, cutting descriptions (GWR*), sonic log, resistivity** (LfU****)
Geretsried GEN-01	GEN	3,682,222	5,306,521	Mud weight, tops, pressure data, drilling events, VSP, DST (Drews et al., 2020b)
Grambach 1	Gra	3,651,824	5,293,177	Mud weight (log header), tops, pressure data, cutting descriptions (GWR*), VSP, sonic log, GR** (LfU****)
Hindelang 1	Hin	3,604,616	5,262,488	Mud weight, tops, pressure data, cutting descriptions (GWR*; Müller, 1995; Müller et al., 1988), VSP, sonic log, GR* (LfU****)
Immenstadt 1	Imm	3,592,870	5,271,240	Mud weight (log header), tops, pressure data, cutting descriptions (GWR*), VSP, sonic log, resistivity** (LfU****)
Kempen 1/1a	Kem	3,608,780	5,284,728	Mud weight, tops, Kicks (EOWR****), VSP, sonic log, GR** (LfU****)
Miesbach 1 (1.)	Mie	3,712,678	5,299,083	Mud weight (Müller et al., 1988), tops, pressure data, cutting descriptions (GWR*), VSP, sonic log, GR** (LfU****)
Murnau 1	Mu1	3,668,814	5,288,295	Mud weight (log header), tops, cutting descriptions (GWR*), VSP (LfU****)
Murnau 2	Mu2	3,665,962	5,290,837	Mud weight (log header), tops, cutting descriptions (GWR*), VSP, sonic log, GR** (LfU****)
Oberhof 1	Ob	3,693,201	5,295,533	Mud weight (log header), tops, pressure data, cutting descriptions (GWR*), VSP, sonic log, GR** (LfU****)
Opfenbach 1	Opf	3,563,310	5,276,740	Mud weight (log header), tops, pressure data, cutting descriptions (GWR*), VSP, sonic log, resistivity** (LfU****)
Schongau 1	Sch	3,651,010	5,302,504	Mud weight (log header), tops, pressure data, cutting descriptions (GWR*), VSP (LfU****)
Seeg 1	See	3,616,796	5,282,005	Mud weight, tops, pressure data (EOWR****), sonic log, GR** (LfU****)
Staffelsee 1	Sta	3,666,001	5,289,953	Mud weight, tops, pressure data, cutting descriptions (GWR*; Müller, 1970; Müller et al., 1988), VSP, sonic log, resistivity** (LfU****)
Sulzberg 1	Sul	3,571,658	5,266,868	Mud weight, tops (Müller et al., 1988)
Vagen 1	Vag	3,715,317	5,306,441	Tops, cutting descriptions (GWR*), VSP, sonic log, resistivity** (LfU****)

\*geological well report; \*\*shale discriminator; \*\*\* Environmental Agency Bavaria; \*\*\*\*end of well report.

outlier readings and small-scale lithological variations.

In the case where neither density nor velocity data are available, a density profile can be estimated using an Athy-type porosity decay function (Athy, 1930) modified for vertical effective stress  $\sigma'_v$  (Heppard et al., 1998; Hubbert and Rubey, 1959; Scott and Thomsen, 1993):

$$\varphi = \varphi_0 \cdot \exp(-\sigma'_{v,hyd} / C) \quad (6)$$

where  $\varphi$  and  $\varphi_0$  are the porosity at vertical hydrostatic effective stress  $\sigma'_{v,hyd}$  and at the surface, respectively.  $C$  is a compaction constant and typically set to  $31 \text{ MPa}^{-1}$  in the study area according to Drews et al. (2018a) and Drews et al. (2019). In combination with an estimate of grain density and pore water density, the resulting porosity profile can be converted into a bulk density profile.

### 5.1.2. Calibration of $\varphi_0$ to model vertical stress and related bulk sediment compaction

In combination with constant grain and fluid densities and assuming hydrostatic pore pressure, equation (6) can be used to model a density profile which can be integrated to a vertical stress profile (equation (4)). In order to investigate the combined effect of lithological composition and compaction on vertical stress we fit equation (6) to data-derived vertical stress profiles by iteratively solving for  $\varphi_0$ . Thereby,  $C$  is kept constant at  $31 \text{ MPa}^{-1}$ . The process is iterative, because no-data intervals are filled with a density estimate that results from equation (6) and constant grain and fluid densities, using the following workflow:

- 1) Employ Gardner's density-velocity relationship (Gardner et al., 1974) to convert velocity data into density data.
- 2) Fill no-data gaps of the resulting velocity-based density profile with a modelled density, using equation (6) with  $C = 31 \text{ MPa}^{-1}$  and matrix and fluid densities of  $2.7$  and  $1.0 \text{ g/cm}^3$ , respectively.
- 3) Integrate the resulting vertical density profile to a vertical stress profile (equation (4)) represented in EMW (equation (1)).
- 4) Model a vertical density profile using equation (6) with  $C = 31 \text{ MPa}^{-1}$  and matrix and fluid densities of  $2.7$  and  $1.0 \text{ g/cm}^3$ , respectively.
- 5) Integrate the resulting density model to a vertical stress profile (equation (4)) represented in EMW (equation (1)).
- 6) Iteratively solve for  $\varphi_0$  in steps 2) and 4) until the vertical stress profiles represented in EMW and generated in steps 3) and 5) have a minimum least square difference.  $\varphi_0$  is identical in steps 2) and 4).

The resulting  $\varphi_0$  represents the best fit vertical stress model and is a measure for the overall compaction state and lithological composition at the respective well location.

## 5.2. Pore pressure analysis

Pore pressure is analyzed on a well-by-well basis. We integrate drilling indicators such as drilling/logging mud weights in combination with mud gas readings, pressure tests (e.g. wireline formation tests and/or drill stem tests) as well as kill mud weights or shut-in drill pipe pressures during reported kick control incidents. In addition, we consider shale pore pressure estimated from velocity data using Eaton's pore pressure transform (Eaton, 1972, 1975):

$$u = \sigma_v - \sigma'_{v,hyd} \cdot \left( \frac{V_{p,obs.}}{V_{p,NCT}} \right)^3 \quad (7)$$

where  $V_{p,obs.}$  is the observed shale velocity and  $V_{p,NCT}$  is the expected shale velocity at a given vertical hydrostatic effective stress  $\sigma'_{v,hyd}$ . The observed shale velocity is derived from sonic log data by either employing a gamma ray (variable) and/or deep resistivity ( $<10 \text{ } \Omega \text{ m}$ ) cut-off (cf. Table 1 for an overview of used shale discriminators for each well) or from VSP data in combination with cutting descriptions.

Drews et al. (2018a) constrained  $V_{p,NCT}$  to velocity data of hydrostatically pressured shales in the NAFB (Fig. 4) by combining equation (6) and a porosity-velocity transform for shales (modified from Raiga-Clemenceau et al., 1986):

$$V_{p,NCT} = 5076 \text{ m/s} \cdot (1 - \varphi_{shale})^2 \quad (8)$$

Where  $\varphi_{shale}$  is the shale porosity, and, according to Drews et al. (2018a) can be computed as follows in the NAFB (cf. equation (6)):

$$\varphi_{shale} = 0.4 \cdot \exp(-\sigma'_{v,hyd} / 31) \quad (9)$$

The resulting normal compaction trend for shale velocity uses vertical effective stress as a proxy for sediment compaction and should thus only yield reasonable results where overpressure is primarily generated by vertical loading. Application of this methodology to velocity data in a fold-and-thrust-belt setting should therefore provide insights on the impact of horizontal loading, uplift and erosion on compaction and overpressure generation.

### 5.3. Extraction of overpressure and velocity-vertical effective stress pairs

Overpressure is extracted from either measured pore pressures (drill stem tests, wireline formation tests, kicks or kill mud weights) or maximum pore pressure estimates per stratigraphic unit. The latter also considers general drilling/logging mud weights and shale pore pressure estimated from velocity data.

Vertical effective stress is derived from pore pressure and vertical

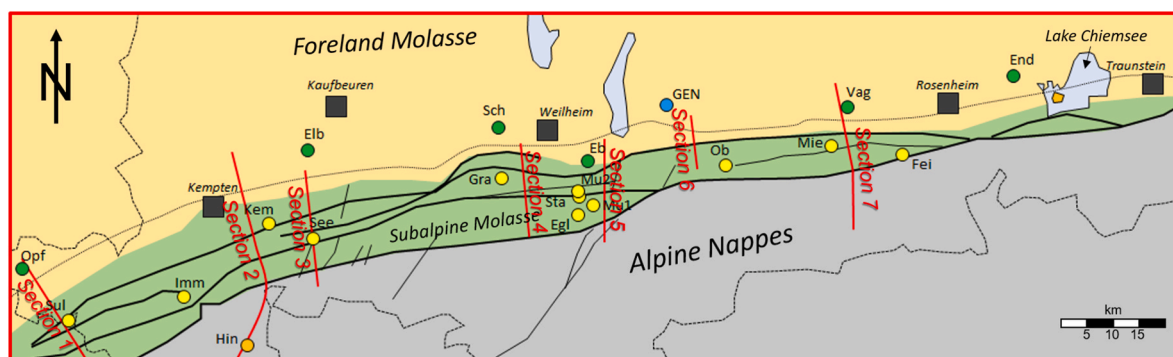


Fig. 3. Map of the study area along the North Alpine Thrust Front in SE Germany (simplified from Ortner et al., 2015) (see red-dashed rectangle in Fig. 1A for regional position). Blue and green dots represent hydrocarbon and geothermal wells, respectively, with surface location in the Foreland Molasse. Yellow dots show the surface location of wells in the Subalpine Molasse (see Table 1 for full well names). Black lines indicate major faults, the grey dashed line marks the northern limit of the Tilted Molasse (cf. Ortner et al., 2015). The dotted black line in the south marks the German-Austrian Border. (For interpretation of the references to color in this figure legend, the reader is referred to the Web version of this article.)

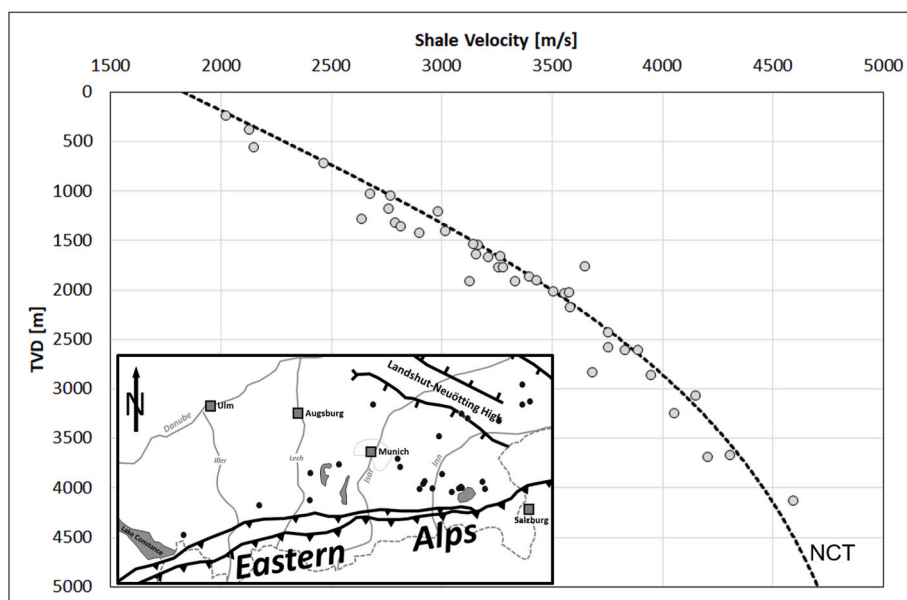


Fig. 4. Normal compaction trend (NCT, black dashed line) for velocity data of hydrostatically pressured shales located in the North Alpine Foreland Basin (modified from Drews et al., 2018a). The inset indicates the surface locations of the wells from which velocity data of hydrostatically pressured shales has been retrieved. TVD = true vertical depth below ground level.

stress estimates of all wells with velocity data (cf. Table 1). Hereby, pore pressure profiles for each well are guided by its available pore pressure indicators. In order to account for the uncertainty related to unresolvable lithological variations, shale velocity and estimated vertical effective stress data pairs are derived by employing two different methodologies:

- 1) Gamma ray or deep resistivity guided filtering of sonic logs for shale-rich sequences and subsequent averaging by using a 30 m moving window. The resulting average shale velocity profiles are directly displayed versus estimated vertical effective stress.
- 2) Computing arithmetic averages of velocity data and vertical effective stress estimates from the clay-rich Oligocene age formations only for each well.

## 6. Results

### 6.1. Bulk sediment compaction and modelled vertical stress

The inferred initial porosity ( $\varphi_0$ , equation (6) and workflow

described in section 5.1.2) indicates that sediments are more densified (lower  $\varphi_0$ ) within the wedge at a given depth than outboard in the foredeep (Fig. 5A). Thereby,  $\varphi_0$  decreases as a function of distance to the NATF when starting from in front of the wedge (Fig. 5A). In addition,  $\varphi_0$  also decreases from East to West in front of the wedge (Fig. 5B). However, behind of the NATF,  $\varphi_0$  is always lower, when compared to locations in front of the NATF at similar Easting (Fig. 5B).

The observed densification trends are most likely impacted by different factors: An eastward change of the depositional environment of Foreland Molasse sediments towards a more marine setting (cf. Kuhlmann and Kempf, 2002) and the onset of overpressure (cf. Drews et al., 2018a) reflect an increase in clay content and probably undercompaction from West to East and thus densification in the opposite direction. However, since the same lithological variations are present within the Subalpine Molasse (Ortner et al., 2015), the densification (decreasing  $\varphi_0$ ) towards and within the wedge most likely indicates an increase of compaction either due to uplift/erosion, horizontal loading or a combination of both processes. We would like to point out that these findings are in concordance with and expand the preliminary work by

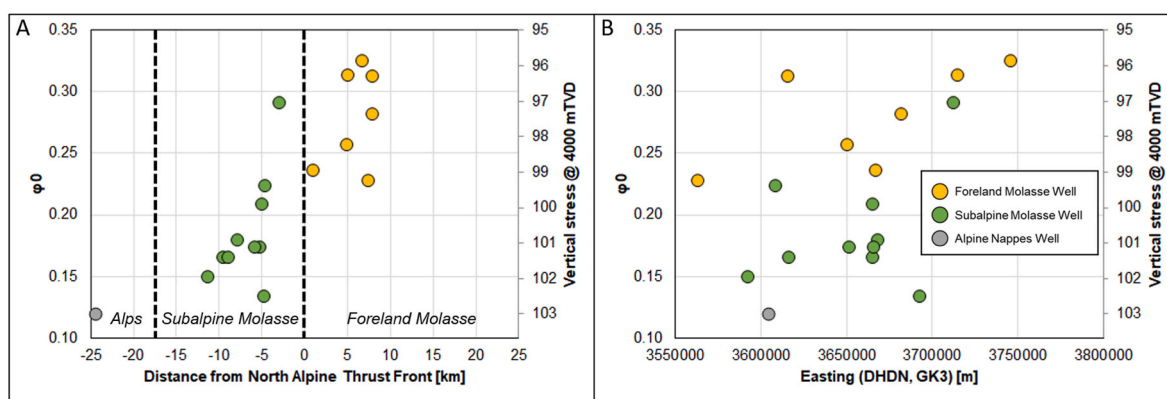


Fig. 5. Calibrated surface porosity  $\varphi_0$  and modelled vertical stress (in MPa) at all well locations where sufficient velocity data were available. A: Variation of  $\varphi_0$  and vertical stress at a depth of 4000 m as a function of well distance to the North Alpine Thrust Front. Negative distances indicate wells are located behind (southward) of the North Alpine Thrust Front. B: Variation of  $\varphi_0$  and vertical stress at a depth of 4000 m as a function of geographical Easting.

Lohr (1969, 1978), who noted a general increase of seismic velocities towards the Alps.

Finally, the resulting initial porosities  $\varphi_0$  can be used to model vertical stress (equations (4) and (6), in combination with constant grain and fluid densities of 2.7 g/cm<sup>3</sup> and 1.0 g/cm<sup>3</sup>, respectively). Analogous to the decrease of  $\varphi_0$ , vertical stress then increases towards and into the wedge (Fig. 5A). Hereby, vertical stress could be up to 7 MPa higher at a depth of 4 km within or below the wedge when compared to vertical stress at the same depth in front of the wedge (Fig. 5A and B).

## 6.2. Pore pressure distribution

### 6.2.1. Pore pressure in front of the wedge: Mesozoic passive margin sediments and Foreland Molasse (foredeep)

Although the investigated wells in front of the wedge are in a distance <10 km to the NATF (cf. Fig. 5A), the relative pore pressure distribution generally follows previous pore pressure studies in front of the wedge (Fig. 6) (Drews et al., 2018a; Lemcke, 1976; Müller et al., 1988).

The Mesozoic Passive Margin Carbonates of early Cretaceous and late Jurassic age are generally (sub-)hydrostatically pressured, as previously reported by Lemcke (1976). Overpressure in Upper Cretaceous and Oligocene shales is increasing from West to East, with hydrostatic pore pressure in the very Western part of the study area (Fig. 6). In the East, pore pressure in front of the wedge exceeds 2.0 g/cm<sup>3</sup> in EMW in Upper Cretaceous and Oligocene shales (see Vagen 1 and Endorf 2 wells in Fig. 6). Previously, such magnitudes have only been observed by maximum drilling mud weights (Müller and Nieberding, 1996; Müller et al., 1988) and can now be confirmed by additional drilling, pore pressure and velocity data.

Moreover, not only the magnitude of overpressure is increasing from West to East, but also the vertical thickness of the overpressured zone (Fig. 6). This can be explained with significantly thicker Chattian, Rupelian and Upper Cretaceous shale packages in the East of the study area (cf. Bachmann et al., 1987; Kuhlemann and Kempf, 2002). Upper Cretaceous shale thickness decreases from >500 m in the East to less than <100 m in the central part and Cretaceous sediments are completely missing in the western part of the study area (Fig. 6). The effect of Upper Cretaceous thickness is also underpinned by a shallower onset of the pore pressure regression in wells with a significantly thinner Upper Cretaceous section (cf. Geretsried GEN-1 well in Fig. 6) which is in agreement with earlier studies by Drews et al. (2018a) and Drews et al. (2020b).

### 6.2.2. Pore pressure within the wedge: Subalpine Molasse

In contrast to the overpressure trend in front of the wedge, overpressure is decreasing from West to East in the Subalpine Molasse (Fig. 6). Shale velocity data often yields an underestimate of shale pore pressure within the wedge, when using a vertical effective stress based compaction trend and pore pressure transform (cf. equations (7)–(9); Fig. 6).

Within surface connected thrust sheets of the western Subalpine Molasse, significant overpressure only builds up within clay-rich formations. For example, very high overpressure is encountered in the Immenstadt 1 well location while hydrostatic pore pressure prevails along the Seeg 1 well (Figs. 6 and 7). Nevertheless, the exact structural position of the Immenstadt 1 well is not known, since the well has been projected on section 2 (cf. Fig. 3). However, other studies addressing the deformation style of this area also project the Immenstadt 1 well behind the triangle zone (e.g. Zerlauth et al., 2014).

Presence of overpressure in the duplexes and/or triangle zone yields pore pressures in excess of 2.0 g/cm<sup>3</sup> in EMW (cf. Sulzberg 1 and Kempton 1/1a on Figs. 6 and 7). In particular, two kicks in the same lithostratigraphic unit in the Kempton 1 and 1a wells, but from different thrust sheets of the triangle zone, yield overpressure magnitudes of 34 MPa at 3380 m and 47 MPa at 4160 m, respectively (Fig. 7, section 2). These very high overpressure kicks provide direct evidence of the

extreme pore pressure contrast between the overpressured wedge and its hydrostatically pressured foredeep in the western part of the study area (cf. Elbsee 1 on Figs. 6 and 7).

In the central and eastern part of the Subalpine Molasse, the triangle zone is less expressed or missing (Fig. 8), because emergent forethrusts take up almost all shortening and the triangle zones were abandoned before they could grow large. Only intermediate overpressure (1.4–1.6 g/cm<sup>3</sup> in EMW) can be observed in these isolated duplexes (cf. Grambach 1 well on Figs. 6 and 8) and in Oligocene age shales of the surface connected thrust sheets (cf. well data in the Subalpine Molasse eastwards of Kaufbeuren on Figs. 6 and 8).

### 6.2.3. Pore pressure below the wedge (footwall): subducted Mesozoic passive margin sediments and subducted Foreland Molasse

In contrast to their counterparts in front of the wedge, subducted Mesozoic Passive Margin Carbonates (Lower Cretaceous and Upper Jurassic) below the Subalpine Molasse can be significantly overpressured (Figs. 6–8), although a pressure regression is usually still observable (cf. Sulzberg 1 and Miesbach 1 wells, Fig. 6).

The subducted parts of the Foreland Molasse (Oligocene shales) and Upper Cretaceous shales are always highly overpressured with pore pressures that translate to EMWs between 1.8 and 2.3 g/cm<sup>3</sup> (Fig. 6). Also, estimated shale pore pressure from velocity data yields a good match with observed pore pressure magnitudes (Fig. 6). However, some uncertainty is related to the pore pressure magnitudes around the basal detachment in the central part of the study area. Here, pressure might drop below the basal detachment to increase again in the fairly thick subducted Foreland Molasse where it converges towards lithostatic stress. This possible pressure inversion is usually highlighted by a discrepancy between pore pressure indicators from drilling data and velocity data (cf. question marks of Grambach 1, Staffelsee 1 and Oberhof 1 wells on Fig. 6) and could be related to shear enhanced compaction in the detachment. However, these inconsistencies require further investigation, for example pore-scale analysis of core samples from the detachment and/or numerical modelling of deformation-driven compaction along the NATF.

### 6.2.4. Regional overpressure trends within, below and in front of the wedge

In the study area, an upper limit overpressure  $u_{\max}^*$  increases linearly with TVD (black dotted line in Fig. 9A):

$$u_{\max}^* = 0.0194 \frac{\text{MPa}}{\text{m}} \cdot \text{TVD} - 33.47 \text{MPa} \quad (10)$$

Compared to the foredeep, overpressure onsets at shallower depths within the wedge (Fig. 9B). Pore fluids within the wedge are supporting up to 60% of the vertical overburden load at 3000 m and more than 70% below 4000 m (Fig. 9B). The shallowest onset of overpressure is within shales of the forethrusts at depths below 2000 m. Below 3000 m, overpressure also reaches the maximum overpressure trend ( $u_{\max}^*$ , equation (10)) in the triangle zone and duplex thrusts (Fig. 9B). In front and below the wedge, overpressure is approaching  $u_{\max}^*$  below 4000 m. Within Mesozoic Passive Margin Carbonates, overpressure can also be observed below 4000 m and quickly converges towards  $u_{\max}^*$  at depths >5000 m (Fig. 9B).

Based on  $u_{\max}^*$ , a range of  $\lambda_{\max}^*$  can be calculated. The range results from variable  $\varphi_0$  used to model vertical stress (cf. Fig. 5), which is required to calculate  $\lambda^*$  (cf. equation (3)). Interestingly,  $\lambda_{\max}^*$  extrapolates to values > 0.95 at depths of 6–8.5 km, when speculating that  $u_{\max}^*$  keeps linearly increasing according to equation (10) (Fig. 9A and B). The resulting depth range correlates with the depth where the basal detachment and post-Mesozoic footwall below the Subalpine Molasse converge towards a subhorizontal dip (cf. Figs. 6–8). Natural seismic focal depths below the Subalpine Molasse roughly coincide with this depth range, too (Department Of Earth And Environmental Sciences, 2001).

### 6.3. Velocity as a function of vertical effective stress in front, within and below the wedge

Cenozoic and Mesozoic shale velocity and average velocity of Oligocene age sediments are investigated as a function of estimated vertical effective stress to assess the role of horizontal loading, uplift and erosion on compaction and overpressure development in front, within and below the wedge (Fig. 10).

Shale velocity from wells located in front of, but very close to, the wedge (Fig. 10A, D) still follows the NCT calibrated to hydrostatically pressured shales in the NAFB. However, a diversion towards faster velocities can also be seen in velocity data of shales, which currently experience a vertical effective stress of less than 10 MPa (Fig. 10A). These elevated velocities are mostly related to the shallower sequences of the Upper and Lower Freshwater Molasse, Brackish Molasse and Upper Marine Molasse (cf. Fig. 2), all of which are characterized by alternating sequences of shale, sandstone and carbonate-rich sediments. The resulting heterolithic character complicates the process of consistent shale picking, which is likely the reason for higher velocities.

Sediments within the wedge (Subalpine Molasse) have significantly faster velocities (Fig. 10B, D) over a similar range of vertical effective stress when compared to the NCT by Drews et al. (2018a) and shales in front of the wedge (Fig. 10A). With increasing vertical effective stress, the discrepancy between shale velocity in the wedge and in front of the wedge is decreasing (Fig. 10D). However, a clear distinction between horizontal loading and uplift/erosion is not possible on the basis of velocity data only (Fig. 10D).

The present day loading conditions below the wedge follow the same velocity-vertical effective stress trend that has been observed in front of the wedge (Fig. 10C). Shale velocity (subducted Foreland Molasse and Mesozoic Passive Margin Sediments) and average velocity data from Oligocene sediments in the footwall follow the NCT of Drews et al. (2018a) over a large range of vertical effective stresses (Fig. 10C and D).

## 7. Discussion

### 7.1. Overpressure vs vertical loading, uplift/erosion and horizontal loading along the NATF

The heterogeneous pore pressure distribution along the NATF in SE Germany allows for an interpretation of the relative timing of overpressure generation in front, within and below the wedge. In combination with the presented velocity-vertical effective stress relationships, the role of horizontal vs vertical loading in front, within and below the wedge can be assessed.

#### 7.1.1. Overpressure development and loading in front of the wedge

In front of the wedge, velocity data correlates well with vertical effective stress and shale velocity matches the NCT previously established in the NAFB (Drews et al., 2018a) (Fig. 10). Thereby, overpressure in the central and eastern parts matches peak sedimentation and burial rates during late Oligocene and early Miocene times (Drews et al., 2018a; Kuhlemann and Kempf, 2002; Zweigel, 1998). Accordingly, overpressure in front of the wedge can be assumed to be predominantly a result of vertical loading due to rapid subsidence/sedimentation and the presence of thick low-permeability shale packages in the central and eastern parts of the study area. Nevertheless, hydrostatic pore pressure prevailed in the western part in front of the wedge (cf. Fig. 6), which is likely related to the lithological shift towards less clay-rich and more permeable sediments and the absence of Upper Cretaceous shales (cf. Bachmann et al., 1987; Kuhlemann and Kempf, 2002) (cf. Fig. 2).

#### 7.1.2. Overpressure development and loading within the wedge

In the west, overpressure is not present in front of the wedge (cf. Fig. 6), suggesting that significant overpressure has likely never built up in this part of the foredeep. Consequently, the observed significant

overpressure in the western parts of the wedge (cf. Fig. 6) has most likely been generated syntectonically. Even compared to the overpressured parts of the foredeep, overpressure develops with higher magnitudes at shallower depth in the wedge than in front of the wedge (Fig. 9), while velocity does not follow the vertical effective stress trend of the foredeep (Fig. 10). Only below 4000 m overpressure magnitudes match magnitudes in front of the wedge (Fig. 9), which is probably marking the depth where vertical loading also dominates within the wedge. Consequently, mechanisms in addition to vertical loading are contributing to overpressure development within the wedge at depths shallower than 4000 m.

A precise assessment of the possible role of uplift, erosion, horizontal and vertical loading within the wedge would require more detailed analyses, such as pore scale compaction studies of core samples from the wedge. Still, some general conclusions regarding overpressure development and loading within the wedge can be made based on the presented pore pressure and velocity data:

Within the triangle zone and duplex thrusts, uplift/erosion is minimal in comparison to shortening (Fig. 7) and horizontal loading is most likely the key driver of overpressure development.

Within imbricates in the western part of the study area, uplift/erosion can be assumed to amount several 100s–1000 s m, depending on the structural position (Fig. 7). Here, overpressure develops at the shallowest depths in the entire study area (Fig. 9) and uplift/erosion is eventually an additional source of overpressure.

In the central and eastern imbricates of the wedge, pore pressure is less than in front of the wedge (Fig. 6). Excess pore pressure has thus never been developed or has been released during uplift/erosion. Müller et al. (1988) also suggest that bedding parallel pressure release towards the surface along the tilted forethrusts might be a possible cause of reduced or missing overpressure.

#### 7.1.3. Overpressure development and loading below the wedge (subducted Foreland Molasse sediments)

Velocity data indicate that vertical loading is probably dominating below the wedge in the entire study area (Fig. 10). Since hydrostatic pore pressure prevails in front of the western wedge, overpressure in the western footwall (subducted Foreland Molasse), must have also developed syntectonically as a result of rapid vertical loading due to the advancing thrust front. Rapid overthrusting of the western footwall is in agreement with the structural-kinematic model proposed by Ortner et al. (2015). In the central and eastern part of the study area, overpressure below the wedge is probably less influenced by overthrusting, since the sediments have already been overpressured due to fast basin subsidence and high sedimentation rates (Drews et al., 2018a, 2020b) (Fig. 6).

#### 7.1.4. Overpressure development and loading below the wedge (Mesozoic Passive Margin Carbonates)

In addition to rapid vertical loading, overpressure in Mesozoic Passive Margin Carbonates below the wedge is most likely also a result of deteriorated reservoir quality. In front of the wedge, Mesozoic Passive Margin Carbonates normally display exceptional hydraulic properties and connectivity: hydrothermal production from Upper Jurassic carbonates often exceed flow rates of 360 m<sup>3</sup>/h (Agemar et al., 2014a) and the pressure regime is consistently (sub-)hydrostatic, following the hydraulic head of the Danube River - even at depths of 4000 m below ground level (Lemcke, 1976). However, this is not the case for deep geothermal projects which are closest to the NATF. Here, five out of six projects either failed due to poor reservoir quality of the Upper Jurassic carbonates or produce at significantly reduced flow rates (BVG, 2019; Drews et al., 2022; Drews et al., 2020a; Flechtner and Aubele, 2019). Accordingly, a loss of hydraulic connectivity has been observed by a decrease of matrix permeability and porosity of Upper Jurassic carbonates with increasing effective stress (Bohnsack et al., 2020, 2021). Thereby, the role of diagenetically-driven fault sealing could also be a

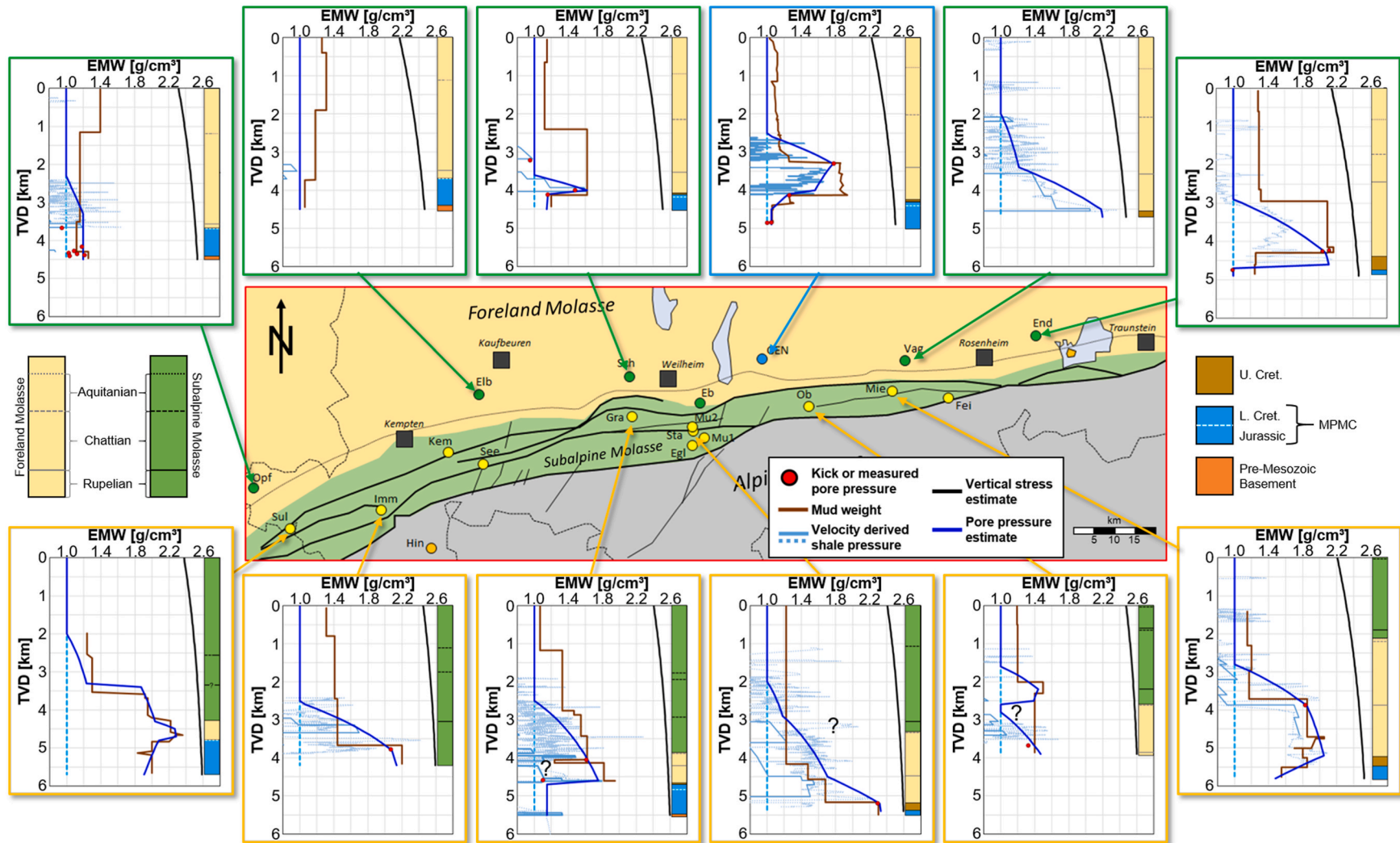


**Fig. 6.** Lateral well-based pore pressure distribution along the North Alpine Thrust Front in equivalent mud weight representation (EMW) vs true vertical depth (TVD) below ground level. Brown lines = drilling/logging mud weights, light blue dashed lines = hydrostatic pressure, solid light blue lines = VSP-derived shale pore pressure estimates, dotted light blue lines = sonic derived shale pore pressure estimates, solid dark blue line = pore pressure interpretation, solid black lines = vertical stress, red dots = measured pore pressure (DST, WLFT or kicks). Question marks indicate sections with high pore pressure uncertainty. Drilling mud weights of Sulzberg 1 (Sul) and Miesbach 1 (Mie) wells from Müller et al. (1988), data of Geretsried GEN-1 well (GEN) from Drews et al. (2020b). Map simplified from Ortner et al. (2015). (For interpretation of the references to color in this figure legend, the reader is referred to the Web version of this article.)

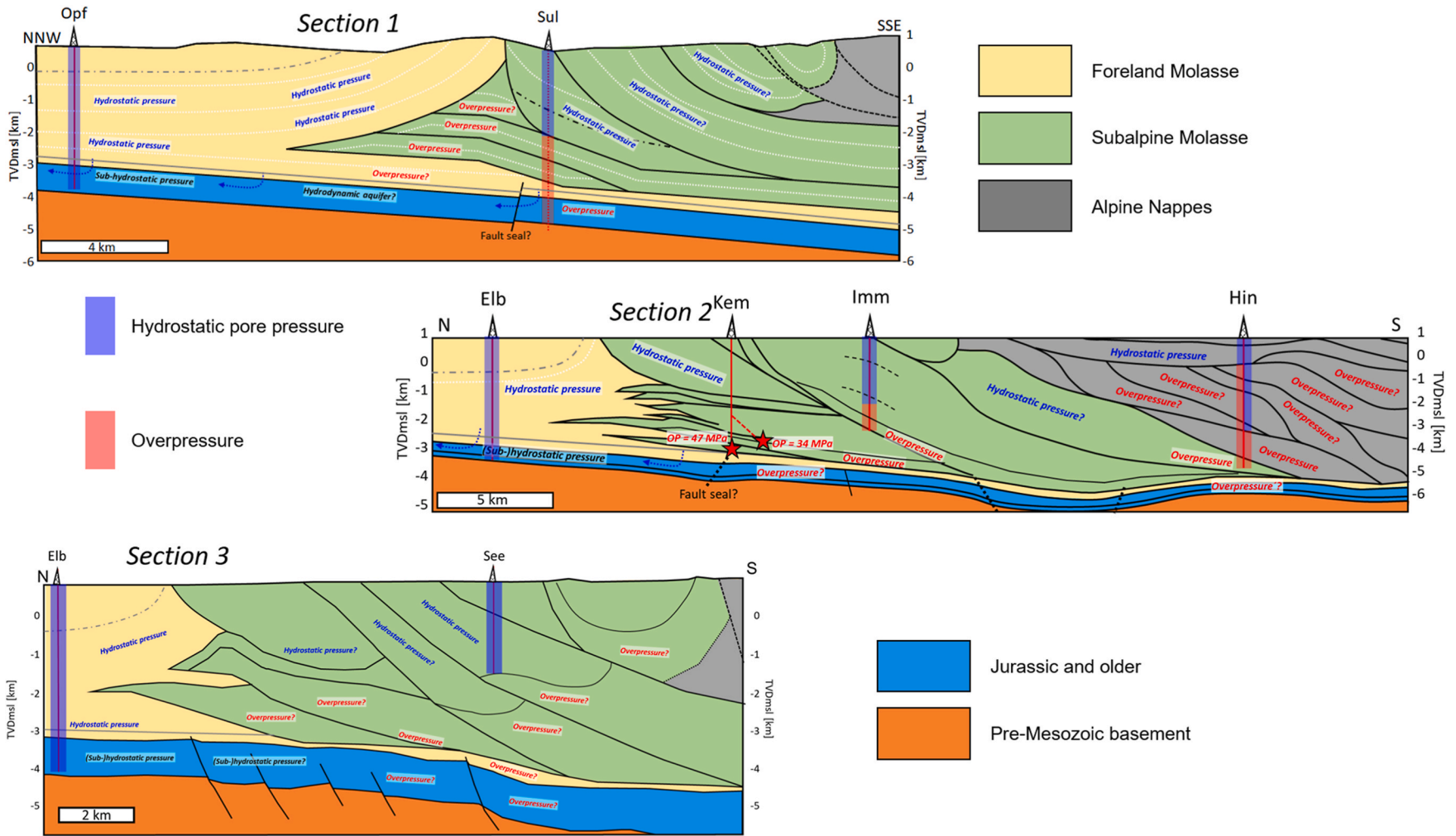


**Fig. 7.** Geologic cross-sections 1–3 with well-based overpressure interpretations (see Fig. 3 for location of cross-sections and Table 1 for full well names). Section 1 adapted after interpretation of Ortner et al. (2015). Northern part (north of projected Immenstadt 1 well) of section 2 adapted after interpretation of Ortner et al. (2015) based on the seismogram from Berge and Veal (2005). Southern part (south of projected Immenstadt 1 well) adapted after Müller (1995). Please note that there is a change in vertical scale due to the stitching of section 2. Section 3 adapted after interpretation of Ortner et al. (2015) based on the seismogram from Schuller et al. (2009). In the Foreland Molasse, grey dashed-dotted lines indicate top Chattian/Aquitanian, grey solid lines represent top Rupelian. Dashed black and thin solid black lines in Subalpine Molasse mark suspected or well-based tops of Chattian or Rupelian, respectively.

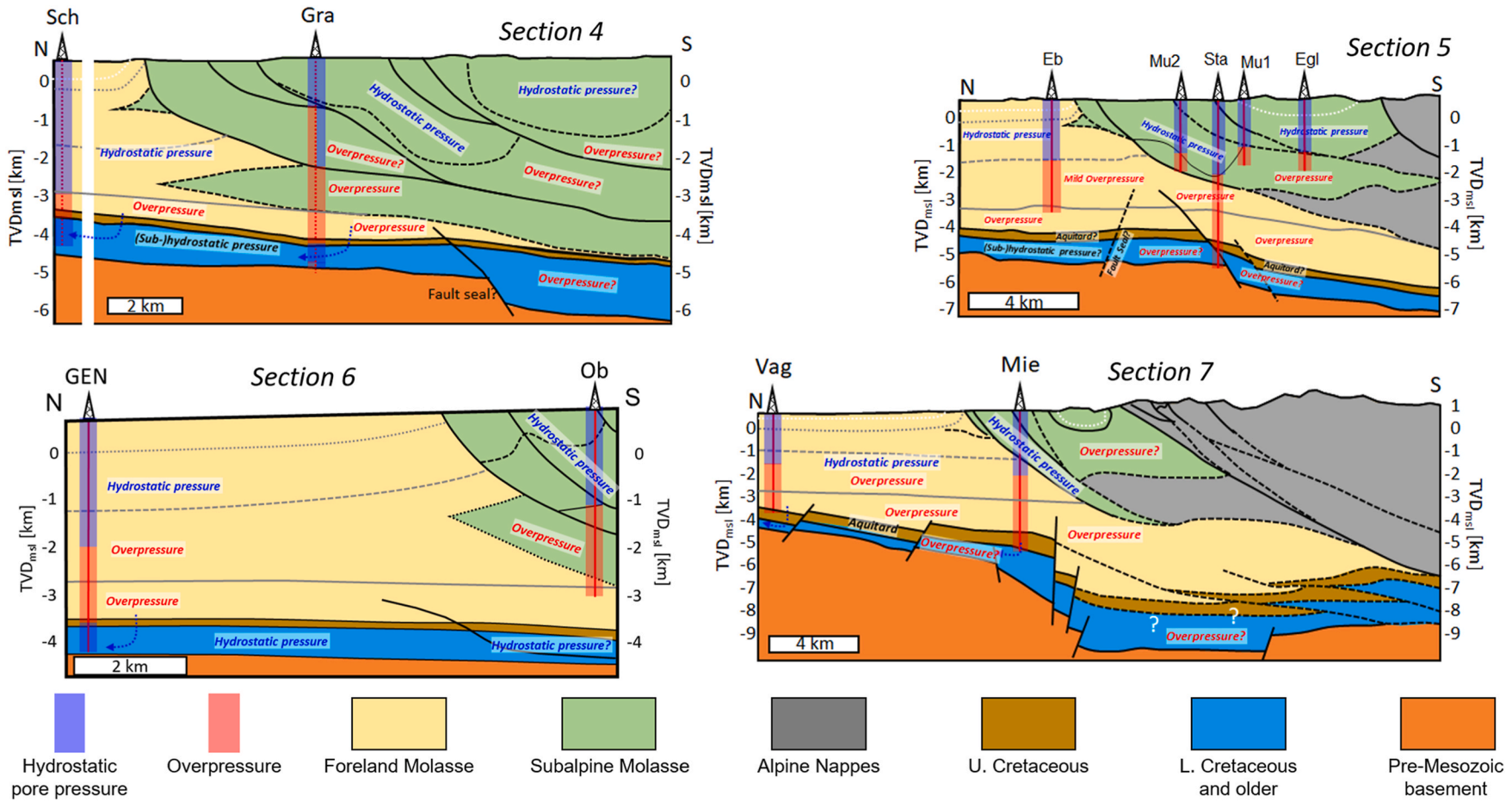


**Fig. 8.** Geologic cross-sections 1–3 with well-based overpressure interpretations (see Fig. 3 for location of cross-sections and Table 1 for full well names). Cross-sections 4–5 adapted after interpretations of Ortner et al. (2015) based on the seismograms from Schuller et al. (2009). Cross-section 6 adapted after Ortner et al. (2015) and Shipilin et al. (2020) and cross-section 7 adapted after Ortner et al. (2015) on the basis of the TRANSALP seismic section (cf. Lüschen et al., 2006). Grey dotted, dashed and solid lines indicate top Aquitanian, Chattian and Rupelian, respectively, in the Foreland Molasse. Black dashed and thin solid lines indicate top Chattian or Rupelian, respectively, in the Subalpine Molasse.

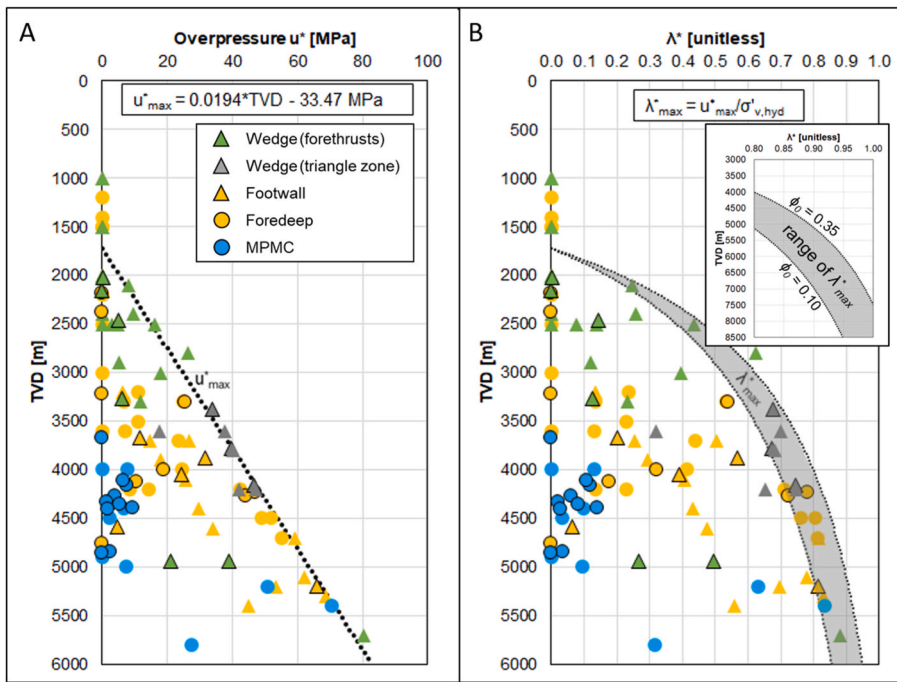


**Fig. 9.** Measured and estimated overpressure as a function of depth. Bordered symbols mark actual measured pressures from drill stem test, wireline formation test or kick data. Data points with borderless symbols have been retrieved from interpreted/ modelled pore pressure, drilling/logging mud weights and vertical stress profiles (cf. Fig. 6). A: Overpressure in MPa vs true vertical depth TVD below ground level. A maximum overpressure trend can be modelled by equation (10) (black dotted line). B: Overpressure expressed as  $\lambda^*$ . The black dotted lines and grey shaded area indicate the range of the maximum overpressure trend constrained in Fig. 9A (see text). The inset shows the range of the maximum overpressure trend, when extrapolated to depths of 6000–8500 m. The legend of Fig. 9A also applies to Fig. 9B. MPMC = Mesozoic Passive Margin Carbonates.

possible mechanism (cf. Figs. 7 and 8).

We therefore speculate that reservoir quality of Mesozoic Passive Margin Carbonates is first reduced by mechanical and chemical

compaction and local fault sealing at depths greater than 4000 m. This self-sealing process might then prevent further hydraulic communication and dewatering towards the Danube River in the north of the NAFB.

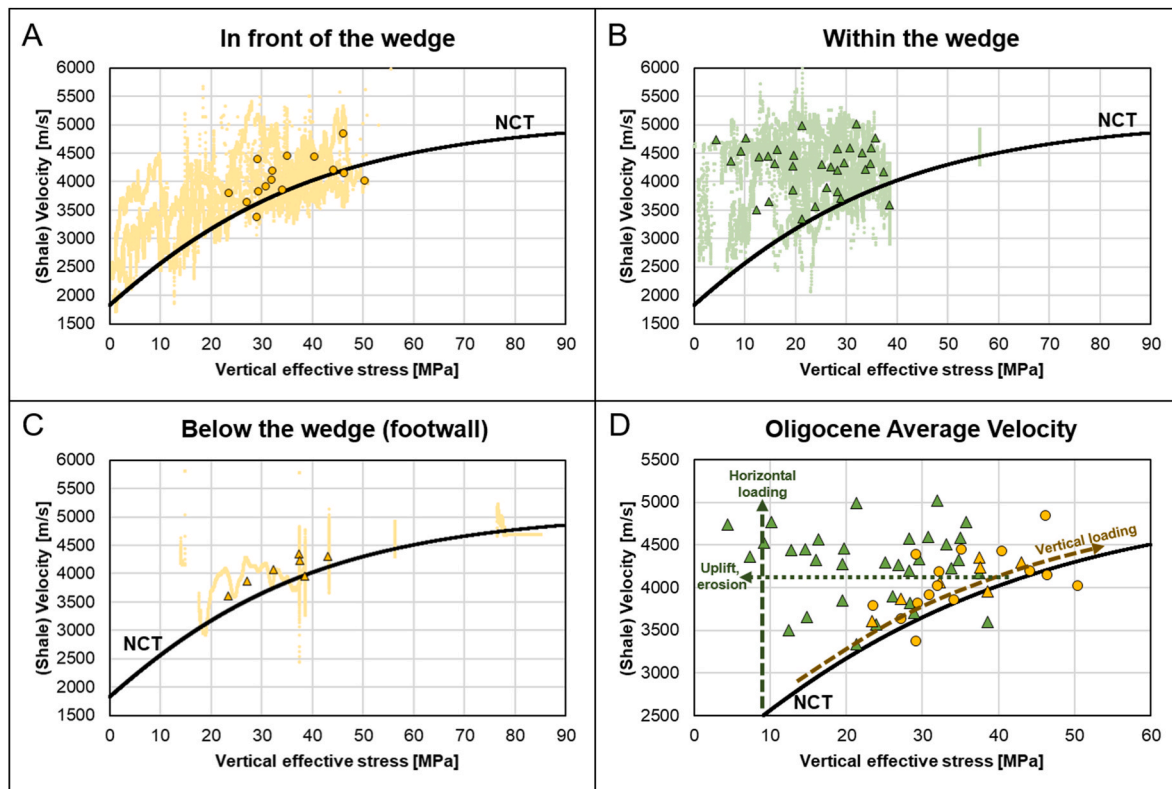


**Fig. 10.** Shale velocity as a function of interpreted vertical effective stress. A–C: Quantitatively derived shale velocity vs vertical effective stress from wells located in front of the wedge (A), within the wedge (Subalpine Molasse) (B) and below the wedge (C). Pale small symbols represent all velocity data filtered for shale-rich sequences using either gamma ray or deep resistivity cut-offs and subsequent 30 m-moving average smoothing. Black-bordered larger symbols show average velocities within Oligocene age formations as a function of interpreted vertical effective stress within Oligocene age formations. The arrows indicate the theoretical impact of horizontal loading, vertical loading, uplift and erosion on velocity and vertical effective stress. NCT = normal compaction trend from Drews et al. (2018a) calibrated to hydrostatically pressured shales in front of the wedge.

Secondly, overpressure possibly develops and quickly converges towards lithostatic magnitudes in the self-sealed carbonates due to the additional and rapidly occurring vertical load of the advancing wedge.

### 7.2. Comparison with other fold-and-thrust-belt systems and implications for the N-S extent of the transition zone between horizontal and vertical loading along the NATF

The above described interpretation of overpressure development and sediment compaction matches the generic loading pattern of other onshore fold-and-thrust-belt and foreland basin systems like the Assam foreland basin in NE India (Dasgupta et al., 2019) or well-studied offshore accretionary prisms such as the Nankai accretionary prism (Flemings and Saffer, 2018; Karig, 1986; Saffer and Tobin, 2011; Tsuji et al., 2008), Sabah fold belt (Couzens-Schultz and Azbel, 2014), Barbados Ridge complex (Bangs et al., 1990; Saffer and Tobin, 2011; Yaolin and Chi-Yuen, 1988) or the Oregon accretionary prism (Cochrane et al., 1994). In all these locations, horizontal loading impacts the wedge, while vertical loading conditions control compaction and overpressure formation in front and below the wedge.

Numerical modelling of fold-and-thrust-belt systems have also reproduced these patterns and also indicate that the transition from wedge conditions (horizontal loading contributes) to far-field conditions in front of the wedge (vertical loading dominates) can span only a few kilometers (Gao et al., 2018; Obradors-Prats et al., 2017). Our study allows us to confirm such a narrow transition zone for onshore fold-and-thrust-belts: all wells in front of the wedge are in a distance of less than 10 km to the NATF and indicate vertical loading is predominant. We therefore propose that the lateral transition zone between horizontal loading and vertical loading conditions along the NATF must be smaller than 10 km and is likely confined to the zone between the northern limits of the Subalpine Molasse and Tilted Molasse (cf. Figs. 2B and 3). This idea is supported by strain analysis based on the deformation of clastic components within Cenozoic conglomerates from different structural elements of the Molasse Basin (wedge – foredeep – forebulge) which indicate a thrust-dominated regime within the wedge and strike-slip or normal faulting regime, respectively, within the Foreland Molasse (Schrader, 1988).

## 8. Conclusions

Overpressure, vertical stress, compaction and horizontal loading along the North Alpine Thrust Front (NATF) have been investigated using drilling and velocity data of 20 wells and previously published interpreted seismic cross-sections.

In general, compaction increases towards and behind the NATF, which results in significant differences of vertical stress magnitudes in front and behind the NATF.

Overpressure is increasing from West to East in front of the wedge and decreases from West to East in the wedge. Below the wedge, overpressure is always present and close to lithostatic stress. Mesozoic Passive Margin Carbonates (Lower Cretaceous and Upper Jurassic), which provide a prolific deep geothermal reservoir in the NAFB and are normally sub-hydrostatically pressured in front of the wedge, can also be overpressured towards and below the wedge, indicating a loss of hydraulic connectivity with increasing depth and vertical effective stress. The onset of overpressure in Mesozoic Passive Margin Carbonates could therefore be a useful indicator for poor reservoir quality and an increased exploration risk, as underpinned by recently failed deep geothermal projects close to the wedge.

The general loading pattern along the NATF matches loading patterns of other onshore fold-and-thrust-belt systems and offshore accretionary prisms: Vertical loading controls compaction and overpressure formation in front and below the wedge. In front of the wedge, vertical loading is most likely related to basin subsidence and sedimentation, whereas below the wedge, vertical loading is mainly due to rapid

overthrusting. Overpressure within the wedge is generated syntectonically by horizontal loading within duplex thrusts and eventually uplift/erosion in imbricates in the western part of the study area, while in the eastern part of the study area, overpressure has either never built up in isolated imbricates of the wedge or dissipated during uplift/erosion. The lateral transition from horizontal loading conditions within the wedge to vertical loading conditions in front of the wedge likely only comprises a few kilometers (<10 km) and probably coincides with the extent of the Tilted Molasse.

In addition to an improved regional understanding of the NATF, and the implications for local deep geothermal exploration, the results of our study also provide a unique reference case for overpressure development in onshore fold-and-thrust-belts and are of relevance to specialists working in the fields of geomechanics, structural geology and geodynamics.

### Data availability

Any raw data used and not disclosed in this study is available upon request from the Bavarian Environmental Agency (Bayerisches Landesamt für Umwelt, Referat Tiefengeologie & Untergrundpotenziale) and the data owners. Processed data is available from the authors upon request.

### Declaration of competing interest

The authors declare that they have no known competing financial interests or personal relationships that could have appeared to influence the work reported in this paper.

### Acknowledgements

This study has been supported by the Bavarian State Ministry of Science and the Arts in the framework of the Geothermal-Alliance Bavaria. The authors would like to thank the data owners of the oil and gas wells Exxon Mobil Deutschland GmbH, OMV E&P GmbH, Neptune Energy Deutschland GmbH and Wintershall Dea Deutschland AG for permission to use and publish their data and BVEG for help and communication regarding the permission process. Special thanks go to Thomas Fritzer from the Bavarian Environmental Agency (LfU) for his kind support during the data acquisition process and to Joachim Wassermann for his input regarding seismic activity along the North Alpine Thrust Front. Last but not least, we would like to thank the reviewers Peter Flemings and Hugo Ortner, who greatly helped to improve the structure and readability and overall quality of the manuscript.

### References

- Agemar, T., Alten, J., Ganz, B., Kuder, J., Kühne, K., Schumacher, S., Schulz, R., 2014a. The geothermal information system for Germany - GeotIS. ZDGG 165, 129–144.
- Agemar, T., Weber, J., Schulz, R., 2014b. Deep geothermal energy production in Germany. *Energies* 7, 4397–4416.
- Allen, P.A., Allen, J.R., 2013. *Basin Analysis: Principles and Application to Petroleum Play Assessment*, third ed. Wiley-Blackwell.
- Athy, L.F., 1930. Density, porosity and compaction of sedimentary rocks. *AAPG (Am. Assoc. Pet. Geol.) Bull.* 14, 1–24.
- Bachmann, G.H., Koch, K., Müller, M., Weggen, K., 1981. Ergebnisse und Erfahrungen bei der Exploration in den Bayerischen Alpen. *Erdoel-Erdgas-Zeitschrift* 97, 127–133.
- Bachmann, G.H., Müller, M., 1996. Die Entwicklung des süddeutschen Molassebeckens seit dem Variszikum: eine Einführung. *Z. Geol. Wiss.* 24, 3–20.
- Bachmann, G.H., Müller, M., Weggen, K., 1987. Evolution of the Molasse Basin (Germany, Switzerland). *Tectonophysics* 137, 77–92.
- Bangs, N.L.B., Westbrook, G.K., Ladd, J.W., Buhl, P., 1990. Seismic velocities from the Barbados Ridge complex: indicators of high pore fluid pressures in an accretionary complex. *J. Geophys. Res.* 95, 8767–8782.
- Berge, T.B., Veal, S.L., 2005. Structure of the alpine foreland. *Tectonics* 24, 1–10.
- Bohnsack, D., Potten, M., Freitag, S., Einsiedel, F., Zosseder, K., 2021. Stress sensitivity of porosity and permeability under varying hydrostatic stress conditions for different carbonate rock types of the geothermal Malm reservoir in Southern Germany. *Geoth. Energy* 9.

- Bohnsack, D., Potten, M., Pfrang, D., Wolpert, P., Zosseder, K., 2020. Porosity–permeability relationship derived from Upper Jurassic carbonate rock cores to assess the regional hydraulic matrix properties of the Malm reservoir in the South German Molasse Basin. *Geoth. Energy* 8.
- Bowers, G.L., 1995. Pore pressure estimation from velocity data: accounting for overpressure mechanisms besides undercompaction. *SPE Drill. Complet.* 10, 89–95. BVG, 2019. Tiefe Geothermie-Projekte in Deutschland 2019.
- Byrne, T., Fisher, D., 1990. Evidence for a weak and overpressured decollement beneath sediment-dominated accretionary prisms. *J. Geophys. Res.* 95, 9081–9097.
- Cochrane, G.R., Moore, J.C., Mackay, M.E., Moore, G.F., 1994. Velocity and inferred porosity model of the Oregon accretionary prism for multichannel seismic reflection data: implications on sediment dewatering and overpressure. *J. Geophys. Res.* 99, 7033–7043.
- Couzens-Schultz, B.A., Azbel, K., 2014. Predicting pore pressure in active fold-thrust systems: an empirical model for the deepwater Sabah foldbelt. *J. Struct. Geol.* 69, 465–480.
- Dasgupta, S., Chatterjee, R., Mohanty, S.P., Alam, J., 2019. Pore pressure modelling in a compressional setting: a case study from Assam, NE India. *J. Petrol. Geol.* 42, 319–338.
- Department Of Earth And Environmental Sciences, G.O., University Of Munchen, 2001. BayernNetz. International Federation of Digital Seismograph Networks.
- Drews, M., Shatyrbayeva, I., Bohnsack, D., Duschl, F., Obermeier, P., Loewer, M., Flechtner, F., Keim, M., 2022. The role of pore pressure and its prediction in deep geothermal energy drilling – examples from the North Alpine Foreland Basin, SE Germany. *Petrol. Geosci.* 28.
- Drews, M., Shatyrbayeva, I., Duschl, F., 2020a. Influence of overburden pressure and stress on reservoir temperature and productivity, north Alpine Foreland Basin, Germany. In: *Third EAGE Workshop on Pore Pressure Prediction*, pp. 1–5.
- Drews, M., Stollhofen, H., 2019. PPFQ prediction in complex tectonic settings: the North Alpine Thrust Front and Foreland Basin, SE Germany. In: *Second EAGE Workshop on Pore Pressure Prediction Amsterdam*.
- Drews, M.C., Bauer, W., Caracciolo, L., Stollhofen, H., 2018a. Disequilibrium compaction overpressure in shales of the Bavarian Foreland Molasse Basin: results and geographical distribution from velocity-based analyses. *Mar. Petrol. Geol.* 92, 37–50.
- Drews, M.C., Bauer, W., Stollhofen, H., 2018b. Porenüberdruck im Bayerischen Molassebecken. *Erdoel, Erdgas, Kohle* 134, 308–310.
- Drews, M.C., Hofstetter, P., Zosseder, K., Shipilin, V., Stollhofen, H., 2020b. Predictability and mechanisms of overpressure in the bavarian foreland Molasse Basin: an integrated analysis of the geretsried GEN-1 deep geothermal well. *Geoth. Energy* 8, 20.
- Drews, M.C., Seithel, R., Savvatis, A., Kohl, T., Stollhofen, H., 2019. A normal-faulting stress regime in the Bavarian Foreland Molasse Basin? New evidence from detailed analysis of leak-off and formation integrity tests in the greater Munich area, SE-Germany. *Tectonophysics* 755, 1–9.
- Eaton, B.A., 1972. The effect of overburden stress on geopressure prediction from well logs. *J. Petrol. Technol.* 24, 929–934.
- Eaton, B.A., 1975. The Equation for Geopressure Prediction from Well Logs. Fall Meeting of the SPE of American Institute of Mining, Metallurgical, and Petroleum Engineers, Dallas, Texas, p. 11.
- Fjaer, E., Holt, R.M., Horsrud, P., Raen, A.M., Risnes, R., 2008. *Petroleum Related Rock Mechanics*, second ed. Elsevier.
- Flechtner, F., Aubele, K., 2019. A brief stock take of the deep geothermal projects in Bavaria, Germany (2018). In: *PROCEEDINGS, 44th Workshop on Geothermal Reservoir Engineering*. Stanford University, Stanford, California.
- Flemings, P.B., 2021. *A Concise Guide to Geopressure - Origin, Prediction, and Applications*. Cambridge University Press.
- Flemings, P.B., Saffer, D.M., 2018. Pressure and stress prediction in the Nankai accretionary prism: a critical state soil mechanics porosity-based approach. *J. Geophys. Res. Solid Earth* 123, 1089–1115.
- Gao, B., Flemings, P.B., Nikolinaokou, M.A., Saffer, D.M., Heidari, M., 2018. Mechanics of fold-and-thrust belts based on geomechanical modeling. *J. Geophys. Res. Solid Earth* 123, 4454–4474.
- Gardner, G.H.F., Gardner, L.W., Gregory, A.R., 1974. Formation velocity and density - the diagnostic basics for stratigraphic traps. *Geophysics* 39, 770–780.
- Heppard, P.D., Cander, H.S., Eggertson, E.B., 1998. Abnormal Pressure and the Occurrence of Hydrocarbons in Offshore Eastern Trinidad, West Indies. *AAPG Memoir*, pp. 215–246.
- Hubbert, M.K., Rubey, W.W., 1959. Role of fluid pressure in mechanics of overthrust faulting. *Bull. Geol. Soc. Am.* 70, 115–166.
- Karig, D.E., 1986. Physical Properties and Mechanical State of Accreted Sediments in the Nankai Trough, Southwest Japan Arc. *Memoir of the Geological Society of America*, pp. 117–133.
- Kuhlemann, J., Kempf, O., 2002. Post-eocene evolution of the north alpine foreland basin and its response to alpine tectonics. *Sediment. Geol.* 152, 45–78.
- Lemcke, K., 1976. *Übertiefe Grundwasser im süddeutschen Alpenvorland*. Bull. Ver. Schweiz. Pet.-Geologen-Ingenieur 42, 9–18.
- Lemcke, K., 1979. Dreissig Jahre Oel- und Gassuche im süddeutschen Alpenvorland. *Jahresber. Mittl. Oberrheinischen Geol. Vereins* 61, 305–317.
- Lohr, J., 1969. Die seismischen Geschwindigkeiten der jüngeren Molasse im ostschweizerischen und deutschen Alpenvorland. *Geophys. Prospect.* 17, 111–125.
- Lohr, J., 1978. Alpine stress documented by anomalous seismic velocities in the Molasse trough. *Inter Union Comm. Geodyn. Sci. Rep.* 38, 69–71.
- Luo, X., Vasseur, G., 1995. Modelling of pore pressure evolution associated with sedimentation and uplift in sedimentary basins. *Basin Res.* 7, 35–52.
- Lüschen, E., Borrini, D., Gebrande, H., Lammerer, B., Millahn, K., Neubauer, F., Nicolich, R., 2006. Transalp - deep crustal Vibroseis and explosive seismic profiling in the Eastern Alps. *Tectonophysics* 414, 9–38.
- Merrell, M.P., Flemings, P.B., Bowers, G.L., 2014. Subsalt pressure prediction in the Miocene mad dog field, gulf of Mexico. *AAPG (Am. Assoc. Pet. Geol.) Bull.* 98, 315–340.
- Mouchet, J.-P., Mitchell, A., 1989. *Abnormal Pressures while Drilling: Origins, Predictions, Detection Evaluation*. Editions Technip, Paris, France.
- Müller, M., 1970. Das Ergebnis der Bohrung Staffelsee 1 als Grundlage für neue Vorstellungen über Bau und Untergrund der gefalteten Molasse. *Geol. Bavarica* 63, 86–106.
- Müller, M., 1995. Die Tiefbohrung Hindelang 1 (Allgäuer Alpen) - projekt und Durchführung. *Geol. Bavarica* 100, 9–21.
- Müller, M., Nieberding, F., 1996. Principles of abnormal pressures related to tectonic developments and their implication for drilling activities (Bavarian Alps, Germany). In: *Wessely, G., Liebl, W. (Eds.), Oil and Gas in Alpidic Thrustbelts and Basins of Central and Eastern Europe*. EAGE Spec. Pub., pp. 119–126.
- Müller, M., Nieberding, F., Wanninger, A., 1988. Tectonic style and pressure distribution at the northern margin of the Alps between Lake constance and the river inn. *Geol. Rundsch.* 77, 787–796.
- Obradors-Prats, J., Rouainia, M., Aplin, A.C., Crook, A.J.L., 2017. Hydromechanical modeling of stress, pore pressure, and porosity evolution in fold-and-thrust belt systems. *J. Geophys. Res. Solid Earth* 122, 9383–9403.
- Ortner, H., Aichholzer, S., Zerlauth, M., Pilsner, R., Fügenschuh, B., 2015. Geometry, amount, and sequence of thrusting in the Subalpine Molasse of western Austria and southern Germany, European Alps. *Tectonics* 34, 1–30.
- Osborne, M.J., Swarbrick, R.E., 1997. Mechanisms for generating overpressure in sedimentary basins: a reevaluation. *AAPG (Am. Assoc. Pet. Geol.) Bull.* 81, 1023–1041.
- Pfiffner, O.A., 1986. Evolution of the North alpine Foreland Basin in the central Alps. *Foreland Basins* 219–228.
- Raiga-Clemenceau, J., Martin, J.P., Nicoletis, S., 1986. The concept of acoustic formation factor for more accurate porosity determination from sonic transit time data. In: *SPWLA 27th Annual Logging Symposium* 1986.
- Reinecker, J., Tingay, M., Müller, B., Heidbach, O., 2010. Present-day stress orientation in the Molasse Basin. *Tectonophysics* 482, 129–138.
- Saffer, D.M., Tobin, H.J., 2011. Hydrogeology and mechanics of subduction zone forearcs: fluid flow and pore pressure. *Annu. Rev. Earth Planet Sci.* 157–186.
- Schmid, S.M., Fügenschuh, B., Kissling, E., Schuster, R., 2004. Tectonic map and overall architecture of the Alpine orogen. *Eclogae Geol. Helv.* 97, 93–117.
- Schrader, F., 1988. Das regionale Gefüge der Drucklösungsdeformation an Geröllern im westlichen Molassebecken. *Geol. Rundsch.* 77, 347–369.
- Schuller, V., Frisch, W., Herzog, U., 2015. Critical taper behaviour and out-of-sequence thrusting on orogenic wedges - an example of the Eastern Alpine Molasse Basin. *Terra Nova* 27, 231–237.
- Schuller, V., Herzog, U., Peresson, H., 2009. Structural Evolution of the German Apine Molasse Basin. *AAPG Research and Discovery Article*, #90090.
- Scott, D.R., Thomsen, L.A., 1993. A global algorithm for pore pressure prediction. In: *8th SPE Middle East Oil Show and Conference*, Manama, Bahrain, pp. 645–654.
- Shipilin, V., Tanner, C., D., Von Hartmann, H., Moeck, I., 2020. Multiphase, decoupled faulting in the southern German Molasse Basin - evidence from 3-D seismic data. *Solid Earth* 11, 2097–2117.
- Sissingh, W., 1997. Tectonostratigraphy of the north alpine foreland basin: correlation of tertiary depositional cycles and orogenic phases. *Tectonophysics* 282, 223–256.
- Suppe, J., 2014. Fluid overpressures and strength of the sedimentary upper crust. *J. Struct. Geol.* 69, 481–492.
- Swarbrick, R.E., Osborne, M.J., 1998. Mechanisms that Generate Abnormal Pressures: an Overview. *AAPG Memoir*, pp. 13–34.
- Tsuji, T., Tokuyama, H., Costa Pisani, P., Moore, G., 2008. Effective stress and pore pressure in the Nankai accretionary prism off the Muroto Peninsula, southwestern Japan. *J. Geophys. Res. Solid Earth* 113.
- von Hagke, C., Oncken, O., Ortner, H., Cederbom, C.E., Aichholzer, S., 2014. Late Miocene to present deformation and erosion of the Central Alps - evidence for steady state mountain building from thermokinematic data. *Tectonophysics* 632, 250–260.
- Wyllie, M.R.J., Gregory, A.R., Gardner, L.W., 1956. Elastic wave velocities in heterogeneous and porous media. *Geophysics* 21, 41–70.
- Yang, Y., Aplin, A.C., 2004. Definition and practical application of mudstone porosity-effective stress relationships. *Petrol. Geosci.* 10, 153–162.
- Yaolin, S., Chi-Yuen, W., 1988. Generation of high pore pressures in accretionary prisms: inferences from the Barbados Subduction Complex. *J. Geophys. Res.* 93, 8893–8910.
- Zerlauth, M., Ortner, H., Pomella, H., Adrian Pfiffner, O., Fügenschuh, B., 2014. Inherited tectonic structures controlling the deformation style: an example from the Helvetic nappes of the Eastern Alps. *Swiss J. Geosci.* 107, 157–175.
- Ziegler, M.O., Heidbach, O., 2020. The 3D stress state from geomechanical–numerical modelling and its uncertainties: a case study in the Bavarian Molasse Basin. *Geoth. Energy* 8.
- Ziegler, M.O., Heidbach, O., Reinecker, J., Przybycin, A.M., Scheck-Wenderoth, M., 2016. A multi-stage 3-D stress field modelling approach exemplified in the Bavarian Molasse Basin. *Solid Earth* 7, 1365–1382.
- Zoback, M.D., 2007. *Reservoir Geomechanics*. Cambridge University Press.
- Zweigel, J., 1998. Eustatic versus tectonic control on foreland basin fill: sequence stratigraphy, subsidence analysis, stratigraphic modelling, and reservoir modelling applied to the German Molasse basin. *Contrib. Sediment Geol.* 20, X–140.